Signature inversion in doubly odd ^{124}La

H. J. Chantler,[1] E. S. Paul,[1,*] A. J. Boston,[1] M. P. Carpenter,[2] R. Charity,[3] C. J. Chiara,[4,†] P. T. W. Choy,[1] C. N. Davids,[2] M. Devlin,[3,‡] A. M. Fletcher,[5] D. B. Fossan,[4] D. G. Jenkins,[6,§] N. S. Kelsall,[6] T. Koike,[4] D. R. LaFosse,[4] P. J. Nolan,[1] D. G. Sarantites,[3] D. Seweryniak,[2] J. F. Smith,[5] K. Starosta,[4] R. Wadsworth,[6] and A. N. Wilson[6,‖]

[1]*Oliver Lodge Laboratory, University of Liverpool, Liverpool L69 7ZE, United Kingdom*

[2]*Physics Division, Argonne National Laboratory, Argonne, Illinois 60439*

[3]*Department of Chemistry, Washington University, St. Louis, Missouri 63130*

[4]*Department of Physics and Astronomy, State University of New York at Stony Brook, Stony Brook, New York 11794-3800*

[5]*Schuster Laboratory, University of Manchester, Brunswick Street, Manchester M13 9PL, United Kingdom*

[6]*Department of Physics, University of York, Heslington, York Y01 5DD, United Kingdom*

(Received 15 March 2002; published 24 July 2002)

High-spin states have been studied in neutron-deficient $^{124}_{57}La_{67}$, populated through the ^{64}Zn(^{64}Zn,3pn) reaction at 260 MeV. The Gammasphere γ-ray spectrometer has been used in conjunction with the Microball charged-particle detector, the Neutron Shell, and the Argonne Fragment Mass Analyzer, in order to select evaporation residues of interest. The known band structures have been extended and new bands found. Most of the bands are linked together, allowing more consistent spin and parity assignments. Comparison of band properties to cranking calculations has allowed configuration assignments to be made and includes the first identification of the $g_{9/2}$ proton-hole in an odd-odd lanthanum isotope. Two bands have been assigned a $\pi h_{11/2} \otimes \nu h_{11/2}$ structure; the yrast one exhibits a signature inversion in its level energies below $I = 18.5\hbar$, while the excited one exhibits a signature inversion above $I = 18.5\hbar$.

DOI: 10.1103/PhysRevC.66.014311 PACS number(s): 27.60.+j, 23.20.Lv, 21.10.Re

I. INTRODUCTION

Doubly odd nuclei of the mass $A \sim 125$ light rare-earth region exhibit the phenomenon of ''signature inversion'' [1] whereby the expected energetically ''unfavored'' signature component of certain bands actually lies lower in energy than the corresponding ''favored'' component at low spin (e.g., see Ref. [2] and references therein). Specifically, for the yrast $\pi h_{11/2} \otimes \nu h_{11/2}$ configuration the ''favored'' $\alpha = 1$ signature, defining odd-spin levels, only becomes energetically favored at spin $I \gtrsim 18\hbar$. The systematics of the critical ''inversion'' spin have been the subject of several recent studies, e.g., Ref. [3], and this phenomenon is still not fully understood theoretically. The present paper provides new results for ^{124}La, in which signature inversion is indeed evident. Signature inversion also occurs in certain bands of doubly odd nuclei in other mass regions. These include $\pi g_{9/2} \otimes \nu g_{9/2}$ bands of $A \sim 80$ nuclei [4,5], $\pi h_{11/2} \otimes \nu i_{13/2}$ bands of $A \sim 160$ nuclei [6], $\pi h_{9/2} \otimes \nu i_{13/2}$ bands of $A \sim 170$–200 nuclei [3], and recently $\pi g_{9/2} \otimes \nu h_{11/2}$ bands of $A \sim 100$ nuclei [7].

A major problem of many doubly odd nuclei is the lack of rigorous spin and parity assignments, which is usually compounded by the observation of many unlinked bands. Global systematic trends of yrast $\pi h_{11/2} \otimes \nu h_{11/2}$ bands have been used to suggest assignments in $A \sim 125$ nuclei [8], while specific experimental studies often reach different conclusions. In the present paper, several band structures in ^{124}La have been linked together, allowing more consistent relative spin assignments to the bands. Furthermore, absolute spin and parity assignments are inferred through comparison to results from the core-quasiparticle coupling model. A second (excited) $\pi h_{11/2} \otimes \nu h_{11/2}$ band has been established in ^{124}La connected to the first (yrast) $\pi h_{11/2} \otimes \nu h_{11/2}$ band. The yrast $\pi h_{11/2} \otimes \nu h_{11/2}$ structure exhibits a signature inversion below $I = (18.5\hbar)$, while the excited structure exhibits a signature inversion above $I = (18.5\hbar)$. The observation of near-degenerate twin $\pi h_{11/2} \otimes \nu h_{11/2}$ bands has recently been cited as evidence for a new ''chiral'' symmetry breaking in nuclei [9,10]. This occurs for triaxially deformed odd-odd nuclei which rotate aplanar to the angular momenta of the odd particles (proton and neutron) in a left-handed or a right-handed geometrical configuration. In the present case, at least at low spin, the larger energy difference between the bands in ^{124}La, of several hundred keV, is more consistent with expectations for an axially symmetric (prolate) nuclear shape with planar rotation.

Another band, not connected to the other structures in ^{124}La, is assigned a high-K $\pi g_{9/2} \otimes \nu h_{11/2}$ configuration; with $K^{\pi} = 8^{-}$, the bandhead is expected to be isomeric and is associated with the known ''high-spin'' isomer assigned in β-decay studies [11]. Bands built on the $\pi g_{9/2} \otimes \nu h_{11/2}$ configuration have systematically been observed in odd-odd Sb ($Z = 51$) isotopes [12], odd-odd I ($Z = 53$) isotopes [13], and also in the lightest odd-odd Cs ($Z = 55$) isotopes [14,15]. The current band represents the first evidence for such a structure

*Corresponding author. Electronic address: esp@ns.ph.liv.ac.uk

†Present address: Department of Chemistry, Washington University, St. Louis, MO 63130.

‡Present address: Los Alamos National Laboratory, Los Alamos, NM 87545.

§Present address: Oliver Lodge Laboratory, University of Liverpool, Liverpool L69 7ZE, United Kingdom.

‖Present address: Department of Nuclear Physics, Research School of Physical Sciences and Engineering, Australian National University, Canberra ACT 0200, Australia.

in odd-odd La ($Z=57$) isotopes, although the $\pi_{9/2}$ orbital is manifest in neighboring odd-A ^{121,123,125}La isotopes [16–18]. Large quadrupole deformation ($\beta_2 \approx 0.28$) brings the $\pi g_{9/2}$ orbital, which originates below the spherical $Z=50$ shell gap, close to the $Z=57$ Fermi surface. Furthermore, this orbital is a key ingredient of the highly deformed (or ''superdeformed'') configurations ($\beta_2 \geqslant 0.35$) in heavier mass $A \sim 130$, $Z<60$ nuclei [19–26].

II. EXPERIMENTAL DETAILS

High-spin states in $A \sim 125$ nuclei were populated with the ^{64}Zn(^{64}Zn, $x\alpha\, yp\, zn\, \gamma$) fusion-evaporation reaction. In particular, states in doubly odd ^{124}La were populated through the $3pn$ ($x=0$, $y=3$, $z=1$) exit channel. The experiment was performed at the Argonne National Laboratory, using a 260-MeV ^{64}Zn beam supplied by the ATLAS superconducting linear accelerator. The beam was incident on a thin self-supporting zinc target, of nominal thickness 500 μg/cm^2. The Gammasphere γ-ray spectrometer [27], containing 78 HPGe detectors, was used in conjunction with the Microball [28,29] charged-particle detector and the Neutron Shell [30] in order to provide clean exit channel selection by defining the number of evaporated particles (x, y, z). In addition, the recoiling evaporation residues were passed through the Argonne Fragment Mass Analyzer (FMA) [31] and were dispersed according to their mass-to-charge (A/q) ratio. A position-sensitive parallel grid avalanche counter, located at the focal plane, provided the A/q information as well as time-of-flight information.

Events were written to tape if three γ rays were detected in prompt coincidence, or two γ rays plus an event in the Neutron Shell, or two γ rays plus an FMA event; approximately 1.06×10^9 events meeting these criteria were recorded.

A. Evaporation particle detection

The Microball charged-particle detector, consisting of 95 closely packed CsI(Tl) scintillators covering 97% of 4π, was used to determine the number of evaporated alpha particles (x) and protons (y) associated with an event. A combination of pulse-shape-discrimination and zero-crossover-timing techniques was used in the off-line analysis to separate light charged particles—namely, protons, deuterons, and alpha particles—as detailed in Ref. [28].

The Neutron Shell, consisting of 30 liquid-scintillator detectors, replaced the five most forward rings of Gammasphere HpGe detectors and was used to define the number of evaporated neutrons (z) associated with an event. The neutron detectors are also sensitive to γ rays, necessitating neutron-γ discrimination; a combination of time-of-flight neutron-γ discrimination and pulse-shape discrimination was used in the off-line analysis.

B. Other channel-selection techniques

In order to improve the channel selection further, the BGO anti-Compton shield elements of the Gammasphere spectrometer were used as a γ-ray fold and sum-energy selection device. By removing the Hevimet collimators, the front of the BGO suppression shields was exposed, allowing γ rays to strike the shield elements directly. The number of BGO elements firing and their total energy were recorded for each event, providing fold (k) and sum-energy (H) information. By setting off-line software gates on a two-dimensional k-H plot, a significant improvement in the quality of the channel selection was made. Specifically, low k and H values enhanced the four-particle ^{124}La channel.

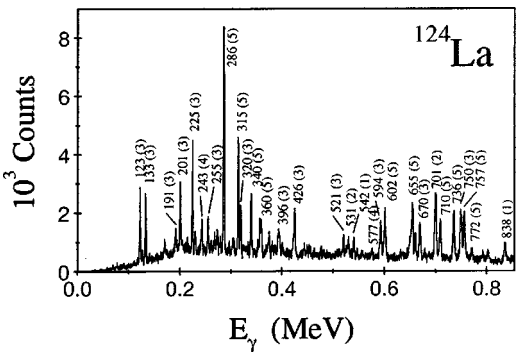

FIG. 1. Gamma rays selected for ^{124}La through a combination of gating techniques as discussed in the text. The transitions are labeled by their energy in keV and band number (Figs. 2 and 3) in parentheses.

Another channel-selection technique consisted in the examination of γ-ray sum energy (H) recorded by Gammasphere in relation to the total energy of the charged particles (E_M) deposited into the Microball. Off-line gates were set on a two-dimensional H-E_M plot [the ''total energy plane'' (TEP) of Ref. [32]] appropriate for ^{124}La. While cutting the overall statistics by a factor of 50, this final selection greatly reduced contamination from ^{125}La ($3p$ channel), the strongest nuclide produced in the ^{64}Zn+^{64}Zn reaction at 260 MeV.

III. RESULTS

Approximately 5.32×10^8 events corresponding to $0\alpha 3p 1n$ evaporation and low k-H were selected from the original data set of 1.06×10^9 events. These selected γ-ray events, of mean fold 3.07, were unfolded into constituent triple (γ^3) coincidence events and replayed into a Radware-format cube [33]; 1.3×10^9 events were incremented into the cube. These selected events were also used for an angular-distribution analysis, as discussed in Sec. III B. In addition, a two-dimensional cut was made on the H-E_M plot to further enhance the ^{124}La channel and a second cube was generated. Approximately 9.8×10^6 events were selected, resulting in 10^8 increments into the second cube. Analysis of the cubes was conducted using the LEVIT8R graphical analysis package [33].

Finally, these events were further gated by the FMA A/q values corresponding to mass 124. The final one-dimensional γ-ray spectrum, with all gating conditions applied, is shown in Fig. 1 and contains essentially only ^{124}La transitions. It should be noted that the γ-ray efficiency is low below 100 keV because absorbers were placed in front of the HPGe detectors to reduce the count rate due to x rays. The presence of the Microball also attenuates the low-energy γ rays.

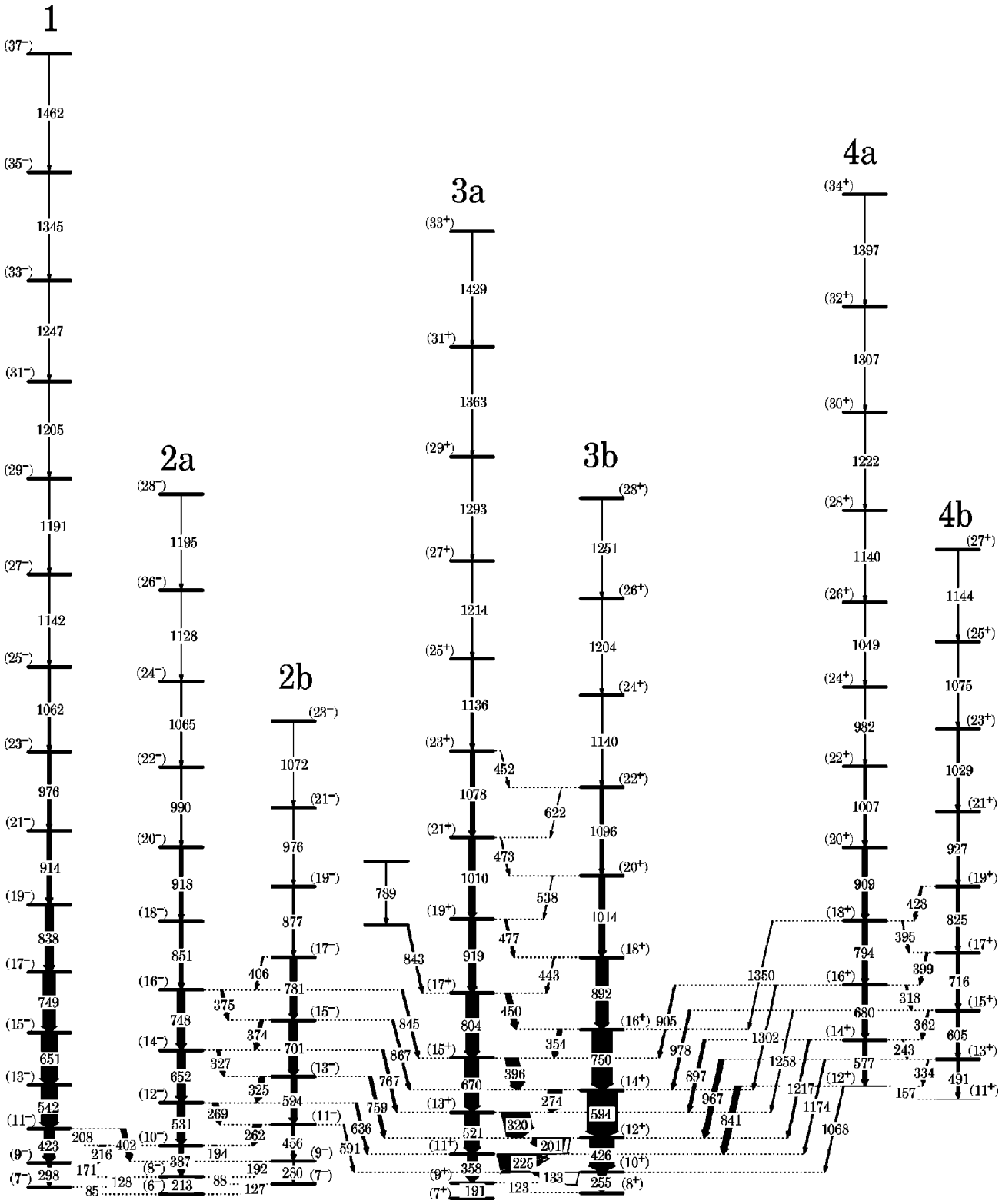

FIG. 2. Level scheme (with Fig. 3) deduced for ^{124}La from this work. The transition energies are given in keV and their relative intensities are proportional to the widths of the arrows.

A. Level scheme construction

The previously known band structure of ^{124}La [34] has been significantly extended. The deduced level scheme of ^{124}La is shown in Figs. 2 and 3, where the ordering of transitions is based on relative γ-ray intensities and triples (γ^3) coincidence relationships. The two parts of the level scheme are unconnected which suggests that the bandhead of band 5

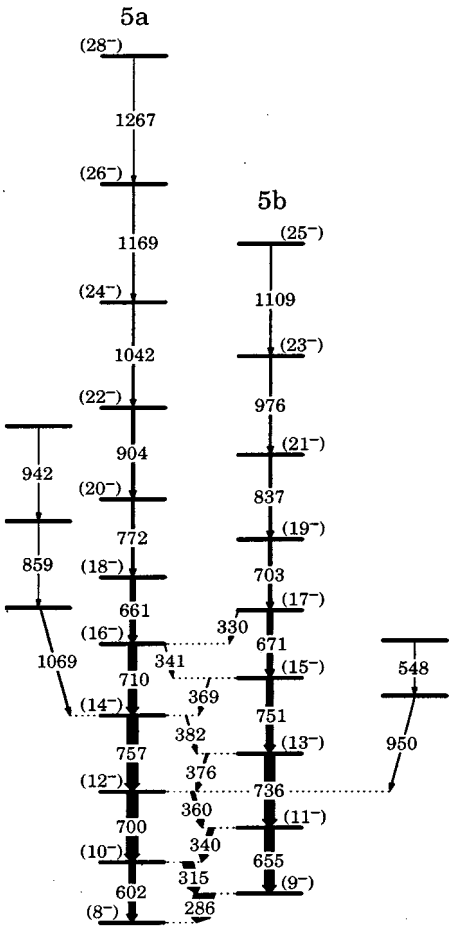

FIG. 3. Level scheme (with Fig. 2) deduced for ^{124}La from this work. The transition energies are given in keV and their relative intensities are proportional to the widths of the arrows.

(Fig. 3) is isomeric. The assignment of $I^{\pi}=K^{\pi}=8^{-}$ to its bandhead follows from the deduced configuration of this band and is consistent with the ''high-spin'' isomer observed in β-decay studies [11]. The measured transition energies and the relative intensities of the ^{124}La γ rays are listed in Tables I–VI. Examples of γ-ray spectra, extracted from the cube, are presented in Figs. 4–6.

B. Relative spin and parity assignments

Although absolute spin and parity assignments cannot be rigorously made from the present experiment; comparison to theory and systematic trends have been used to derive the values given in Figs. 2 and 3, as discussed in Sec. IV A. Relative assignments are, however, inferred from the experiment.

In order to establish multipolarities of the strong transitions, an angular-distribution analysis of the data was performed. After selecting transitions in ^{124}La with the ancillary detectors, the γ-ray data were projected out into the rings of Gammasphere at a given angle θ relative to the beam direction; eight rings were used in this analysis. The normalized transition intensities were determined in each ring and were fitted to the standard Legendre expansion of the angular-distribution function [35],

TABLE I. Measured properties of the γ-ray transitions assigned to band 1.

E_γ (keV)[a]	I_γ[b]	A_2	A_4	R	Mult.	Assignment
298.0	14.3			0.96(3)	$E2$	$(9^-\rightarrow 7^-)$
423.1	48.3			0.96(2)	$E2$	$(11^-\rightarrow 9^-)$
541.5	75.8	0.295(88)	0.148(94)	1.10(2)	$E2$	$(13^-\rightarrow 11^-)$
651.1	73.2			1.01(2)	$E2$	$(15^-\rightarrow 13^-)$
749.2	59.1			1.07(2)	$E2$	$(17^-\rightarrow 15^-)$
837.8	38.2			0.93(2)	$E2$	$(19^-\rightarrow 17^-)$
914.1	19.6			0.97(4)	$E2$	$(21^-\rightarrow 19^-)$
975.6	10.8			1.06(6)	$E2$	$(23^-\rightarrow 21^-)$
1061.7	6.4					$(25^-\rightarrow 23^-)$
1141.6	3.9					$(27^-\rightarrow 25^-)$
1190.6	2.9					$(29^-\rightarrow 27^-)$
1205.0	1.6					$(31^-\rightarrow 29^-)$
1247.0	1.3					$(33^-\rightarrow 31^-)$
1345.1	0.7					$(35^-\rightarrow 33^-)$
1462.4	0.1					$(37^-\rightarrow 35^-)$

[a]The γ-ray energies are estimated to be accurate to ± 0.3 keV for the strong transitions ($I_\gamma > 10$), rising to ± 0.6 keV for the weaker transitions.

[b]Errors on the relative intensities are estimated to be less than 5% of the quoted values for strong transitions ($I_\gamma > 10$) and less than 10% for the weaker transitions.

$$W(\theta)=1+A_2P_2(\cos\theta)+A_4P_4(\cos\theta), \tag{1}$$

in order to obtain empirical A_2 and A_4 angular-distribution coefficients. For some of the weaker transitions, or those with an unphysically large fitted A_4 value, A_4 was set to zero and only a value for A_2 extracted. Examples of the fitted angular distributions are shown in Fig. 7. The angular-distribution coefficients obtained for some of the stronger dipole transitions were used to extract multipole mixing ratios δ by comparing the deduced A_2 and A_4 values to theoretical values [35,36]; the results for transitions in bands 2, 3, and 5, using the phase convention of Ref. [35], are included in Tables II, III, and V, respectively.

Multipolarity assignments for the weaker transitions and doublet transitions were made from an angular-correlation analysis of coincident γ-ray intensities. An average coincident angular-intensity ratio, defined as

$$R=\frac{I_{\gamma\gamma}(\theta_1\approx 50^\circ,130^\circ;\theta_2\approx 90^\circ)}{I_{\gamma\gamma}(\theta_1\approx 90^\circ;\theta_2\approx 50^\circ,130^\circ)}, \tag{2}$$

was evaluated for the transitions. Here the coincident intensities $I_{\gamma\gamma}$ were measured at an angle θ_1 when gated by quadrupole transitions at an angle θ_2. This approach yields theoretical R values for pure stretched quadrupole and pure stretched dipole transitions of approximately 1.00 and 0.63, respectively; these results are included in Tables I–VI.

TABLE II. Measured properties of the γ-ray transitions assigned to band 2.

E_γ (keV) [a]	I_γ [b]	A_2	A_4	δ	R	Mult.	Assignment
87.6	4.4				0.46(8)	$M1/E2$	$(8^-\rightarrow 7^-)$
126.3	10.0				0.55(4)	$M1/E2$	$(7^-\rightarrow 6^-)$
192.5	35.0				0.49(2)	$M1/E2$	$(9^-\rightarrow 8^-)$
194.5	17.9				0.47(2)	$M1/E2$	$(10^-\rightarrow 9^-)$
212.5	5.2						$(8^-\rightarrow 6^-)$
262.0	34.5	$-0.139(70)$	0.105(84)	0.057(4)	0.47(2)	$M1/E2$	$(11^-\rightarrow 10^-)$
269.3	23.6	$-0.565(85)$	$\equiv 0$		0.50(2)	$M1/E2$	$(12^-\rightarrow 11^-)$
279.6	5.9						$(9^-\rightarrow 7^-)$
324.7	20.6				0.41(2)	$M1/E2$	$(13^-\rightarrow 12^-)$
326.9	13.2				0.60(2)	$M1/E2$	$(14^-\rightarrow 13^-)$
373.7	15.2				0.51(2)	$M1/E2$	$(15^-\rightarrow 14^-)$
375.2	8.6				0.51(2)	$M1/E2$	$(16-\rightarrow 15^-)$
386.7	20.1				0.88(3)	$E2$	$(10^-\rightarrow 8^-)$
406.1	5.7						$(17^-\rightarrow 16^-)$
456.0	12.3				0.78(4)	$E2$	$(11^-\rightarrow 9^-)$
531.0	35.2				1.06(2)	$E2$	$(12^-\rightarrow 10^-)$
593.9	25.2	0.320(81)	$-0.016(86)$		0.99(2)	$E2$	$(13^-\rightarrow 11^-)$
651.8	39.8	0.544(66)	$\equiv 0$		0.97(3)	$E2$	$(14^-\rightarrow 12^-)$
700.6	31.0				0.91(3)	$E2$	$(15^-\rightarrow 13^-)$
748.0	33.1				1.16(4)	$E2$	$(16^-\rightarrow 14^-)$
781.2	26.4				1.13(5)	$E2$	$(17^-\rightarrow 15^-)$
851.3	14.5				0.98(5)	$E2$	$(18^-\rightarrow 16^-)$
877.0	7.0				1.63(10)	$E2$	$(19^-\rightarrow 17^-)$
917.7	10.7				1.00(5)	$E2$	$(20^-\rightarrow 18^-)$
975.6	2.6				1.06(6)	$E2$	$(21^-\rightarrow 19^-)$
990.4	4.1				1.14(7)	$E2$	$(22^-\rightarrow 20^-)$
1064.8	3.4						$(24^-\rightarrow 22^-)$
1073.1	1.2						$(23^-\rightarrow 21^-)$
1128.5	1.4						$(26^-\rightarrow 24^-)$
1194.4	0.6						$(28^-\rightarrow 26^-)$

[a]The γ-ray energies are estimated to be accurate to ± 0.3 keV for the strong transitions ($I_\gamma > 10$), rising to ± 0.6 keV for the weaker transitions.

[b]Errors on the relative intensities are estimated to be less than 5% of the quoted values for strong transitions ($I_\gamma > 10$) and less than 10% for the weaker transitions.

C. Band structures in ^{124}La

Bands 1–3 were previously observed in Ref. [34] but no links between bands 2 and 3 were found; no spin or parity assignments were made. These three bands have now been observed to higher spin and linked together, while bands 4 and 5 are newly identified. The current spin and parity assignments start from band 3. This band represents the low-spin yrast configuration and is hence associated with high-j proton and neutron intruder orbitals: namely, $\pi h_{11/2}$ and $\nu h_{11/2}$ orbitals. The $\pi h_{11/2} \otimes \nu h_{11/2}$ configuration is consistent with the assignment of Ref. [34] and also the band's alignment properties.

The coupling of the low-Ω $h_{11/2}$ proton ($\Omega = 1/2$) and high-Ω $h_{11/2}$ neutron ($\Omega = 7/2$) leads to a semidecoupled [37] structure for band 3 with an expected K value of 3 or 4 (i.e., $7/2 \pm 1/2$) at low spin. The spin and parity of the lowest level experimentally determined in this band are, however, tentatively assigned $I^\pi = 7^+$ through comparison to results of the core-quasiparticle coupling model, as discussed in Sec. IV A.

The interlinking dipole and quadrupole transitions between bands 1 and 2 at low spin imply that these bands have the same parity. The transitions linking bands 2 and 3 have angular-correlation values consistent with pure stretched dipole transitions and are assigned as $E1$ transitions. Moreover, the lack of $\Delta I = 2$ links (i.e., $E2$ transitions) also suggests a change in parity. Bands 1 and 2 are hence assigned negative parity. The present assignments for ^{124}La are also consistent with the lowest-energy theoretical $\Delta I = 2$ band (doubly decoupled [38] band 1) having signature $\alpha = 1$, i.e., odd spins.

The observation of both $\Delta I = 1$ and $\Delta I = 2$ transitions linking bands 3 and 4 suggests that they have the same (positive) parity. Indeed, the positive A_2 coefficient for the 841 keV linking transition (Table VI) implies $\Delta I = 1$ $M1/E2$ character with $\delta > 0$ for this transition.

TABLE III. Measured properties of the γ-ray transitions assigned to band 3.

E_γ (keV) [a]	I_γ [b]	A_2	A_4	δ	R	Mult.	Assignment
122.6	63.6				0.61(2)	$M1/E2$	$(9^+\rightarrow 8^+)$
133.2	152.1				0.54(1)	$M1/E2$	$(10^+\rightarrow 9^+)$
191.4	4.2				0.88(6)	$E2$	$(9^+\rightarrow 7^+)$
200.9	147.8	−0.306(60)	0.049(77)	−0.050(12)	0.51(1)	$M1/E2$	$(12^+\rightarrow 11^+)$
225.0	198.7	−0.286(61)	0.081(77)	−0.035(13)	0.55(1)	$M1/E2$	$(11^+\rightarrow 10^+)$
255.4	34.0	0.236(79)	−0.053(95)		1.01(3)	$E2$	$(10^+\rightarrow 8^+)$
274.1	61.2	−0.346(60)	0.081(77)	−0.079(15)	0.51(2)	$M1/E2$	$(14^+\rightarrow 13^+)$
320.0	120.0	−0.401(58)	0.069(75)	−0.113(20)	0.45(1)	$M1/E2$	$(13^+\rightarrow 12^+)$
354.1	19.2	−0.790(66)	0.094(94)		0.48(4)	$M1/E2$	$(16^+\rightarrow 15^+)$
357.9	42.5	0.226(84)	−0.019(94)		1.04(3)	$E2$	$(11^+\rightarrow 9^+)$
396.3	57.0	−0.363(60)	0.075(77)	−0.091(13)	0.42(2)	$M1/E2$	$(15^+\rightarrow 14^+)$
425.6	109.4	0.225(79)	−0.129(86)		1.06(2)	$E2$	$(12^+\rightarrow 10^+)$
442.8	4.2				0.48(5)	$M1/E2$	$(18^+\rightarrow 17^+)$
449.9	23.2	−0.342(60)	$\equiv 0.0$		0.40(4)	$M1/E2$	$(17^+\rightarrow 16^+)$
453.4	0.7				0.34(6)	$M1/E2$	$(23^+\rightarrow 22^+)$
473.4	2.7						$(21^+\rightarrow 20^+)$
476.6	8.3						$(19^+\rightarrow 18^+)$
520.6	64.6	0.519(48)	$\equiv 0.0$		1.00(3)	$E2$	$(13^+\rightarrow 11^+)$
538.0	1.4						$(20^+\rightarrow 19^+)$
593.8	134.3	0.301(81)	−0.028(84)		1.02(4)	$E2$	$(14^+\rightarrow 12^+)$
622.2	1.1						$(22^+\rightarrow 21^+)$
670.2	63.1	0.339(81)	−0.068(85)		1.08(3)	$E2$	$(15^+\rightarrow 13^+)$
750.3	91.4	0.416(84)	0.080(88)		1.08(2)	$E2$	$(16^+\rightarrow 14^+)$
803.8	55.8	0.403(91)	−0.156(96)		1.12(3)	$E2$	$(17^+\rightarrow 15^+)$
892.3	54.0	0.356(95)	−0.202(10)		1.05(4)	$E2$	$(18^+\rightarrow 16^+)$
919.0	32.5	0.409(86)	0.002(90)		1.27(9)	$E2$	$(19^+\rightarrow 17^+)$
1010.0	27.2				1.02(7)	$E2$	$(21^+\rightarrow 19^+)$
1013.9	24.9				0.86(6)	$E2$	$(20^+\rightarrow 18^+)$
1077.5	17.2						$(23^+\rightarrow 21^+)$
1096.1	10.9				1.01(11)	$E2$	$(22^+\rightarrow 20^+)$
1135.6	6.5						$(25^+\rightarrow 23^+)$
1140.0	6.5						$(24^+\rightarrow 22^+)$
1199.9	1.4						$(26^+\rightarrow 24^+)$
1213.9	3.3						$(27^+\rightarrow 25^+)$
1251.1	1.6						$(28^+\rightarrow 26^+)$
1293.3	1.1						$(29^+\rightarrow 27^+)$
1363.2	0.9						$(31^+\rightarrow 29^+)$
1429.3	0.2						$(33^+\rightarrow 31^+)$

[a]The γ-ray energies are estimated to be accurate to ± 0.3 keV for the strong transitions ($I_\gamma > 10$), rising to ± 0.6 keV for the weaker transitions.

[b]Errors on the relative intensities are estimated to be less than 5% of the quoted values for strong transitions ($I_\gamma > 10$) and less than 10% for the weaker transitions.

The use of ancillary detectors with Gammasphere conclusively proves that band 5 belongs to ^{124}La (see Fig. 1]). It is not in prompt coincidence with the other bands of ^{124}La which suggests that the bandhead is isomeric. The band properties are consistent with a high-K ($K^\pi = 8^-$) $\pi g_{9/2} \otimes \nu h_{11/2}$ configuration, and hence the bandhead is assigned $I^\pi = 8^-$. The high-K nature of the bandhead is expected to make this level isomeric; indeed a ''high-spin'' isomer with $I^\pi = 7^-$ or 8^- has been observed in β-decay studies of ^{124}La which populated states in ^{124}Ba up to $I^\pi = 7^-$ and 8^+ [11]. The present configuration assignment is consistent with an 8^- isomeric bandhead for band 5.

IV. DISCUSSION

A. Absolute spin and parity assignments

The core-quasiparticle coupling model (CQPCM) [39–41] has been used to calculate the energy levels of the $\pi h_{11/2} \otimes \nu h_{11/2}$ bands (bands 3 and 4) in ^{124}La. This model has already been successfully applied to this mass region

TABLE IV. Measured properties of the γ-ray transitions assigned to band 4.

E_γ (keV) [a]	I_γ [b]	A_2	A_4	R	Mult.	Assignment
157.1	1.2					$(12^+ \rightarrow 11^+)$
242.6	5.9			0.54(2)	$M1/E2$	$(14^+ \rightarrow 13^+)$
318.2	7.0					$(16^+ \rightarrow 15^+)$
334.0	3.9					$(13^+ \rightarrow 12^+)$
362.4	7.0			0.59(3)	$M1/E2$	$(15^+ \rightarrow 14^+)$
394.8	4.7					$(18^+ \rightarrow 17^+)$
398.6	6.8					$(17^+ \rightarrow 16^+)$
427.9	8.0					$(19^+ \rightarrow 18^+)$
490.7	8.6			1.04(6)	$E2$	$(13^+ \rightarrow 11^+)$
576.9	18.3	0.297(81)	$-0.028(85)$	0.98(2)	$E2$	$(14^+ \rightarrow 12^+)$
605.1	12.1			1.09(4)	$E2$	$(15^+ \rightarrow 13^+)$
680.3	23.6	0.431(71)	$\equiv 0$	0.90(2)	$E2$	$(16^+ \rightarrow 14^+)$
716.1	13.0					$(17^+ \rightarrow 15^+)$
794.2	24.6			0.97(2)	$E2$	$(18^+ \rightarrow 16^+)$
824.7	11.5					$(19^+ \rightarrow 17^+)$
909.2	22.7			1.20(14)	$E2$	$(20^+ \rightarrow 18^+)$
926.8	8.4					$(21^+ \rightarrow 19^+)$
982.2	2.9					$(24^+ \rightarrow 22^+)$
1006.9	11.2			1.18(18)	$E2$	$(22^+ \rightarrow 20^+)$
1029.1	10.6					$(23^+ \rightarrow 21^+)$
1049.2	2.5					$(26^+ \rightarrow 24^+)$
1074.5	3.4					$(25^+ \rightarrow 23^+)$
1140.1	2.3					$(28^+ \rightarrow 26^+)$
1143.8	1.7					$(27^+ \rightarrow 25^+)$
1221.7	2.2					$(30^+ \rightarrow 28^+)$
1307.1	1.3					$(32^+ \rightarrow 30^+)$
1397.1	0.9					$(34^+ \rightarrow 32^+)$

[a]The γ-ray energies are estimated to be accurate to ± 0.3 keV for the strong transitions ($I_\gamma > 10$), rising to ± 0.6 keV for the weaker transitions.

[b]Errors on the relative intensities are estimated to be less than 5% of the quoted values for strong transitions ($I_\gamma > 10$) and less than 10% for the weaker transitions.

[42–44]. In the present case, a triaxial ($\gamma = 13°$) rigid-rotor ^{122}Ba core was first coupled to an odd $h_{11/2}$ neutron to form ^{123}Ba and then to an odd $h_{11/2}$ proton to produce ^{124}La. The results for the first and second $\pi h_{11/2} \otimes \nu h_{11/2}$ configurations are presented in Figs. 8, and 9, respectively, where they are compared to the experimental energy levels of bands 3 and 4. Good agreement is found when the lowest observed level of band 3 is assigned spin $7\hbar$. It should be noted that the theoretical state of spin $5\hbar$ lies only 30 keV below the state of spin $7\hbar$, which may explain why this state was not identified experimentally. With these spin assignments, the energy levels of band 4 are also well reproduced (Fig. 9).

The current assignment of $9^+ \rightarrow 7^+$ for the 191 keV transition of ^{124}La is consistent with the systematics of odd-odd lanthanum isotopes [8] and also recent ''extended'' total Routhian surface (TRS) calculations [45]. In contrast, however, recent work on ^{126}La [46] has suggested spin values $2\hbar$ lower for the $\pi h_{11/2} \otimes \nu h_{11/2}$ configuration in that nucleus, in conflict with the general systematic trend [8].

B. Cranked Woods-Saxon calculations

Representative results of cranked Woods-Saxon calculations for ^{124}La, employing a triaxial Woods-Saxon single-particle potential [47,48], are shown in Fig. 10. In these calculations, the pairing strength is calculated at zero frequency and is modeled to decrease with increasing rotational frequency such that the pairing has fallen by 50% at $\omega = 0.70$ MeV/$\hbar$, as detailed in Ref. [49]. Average deformation parameters $\beta_2 = 0.28$, $\beta_4 = 0.0$, and $\gamma = 0°$ were obtained from standard TRS calculations [49–51] for possible configurations in ^{124}La. The labelling convention of the orbitals is listed in Table VII, together with their calculated g factors [48]

$$g_\Omega = \frac{1}{\Omega}[g_l \langle l_z \rangle + g_s \langle s_z \rangle]. \quad (3)$$

In Eq. (3), g_s is taken as 70% of $g_{s,free}$, while $g_l = 1$ for protons and $g_l = 0$ for neutrons. The calculations are performed over a decomposition of harmonic oscillator basis

TABLE V. Measured properties of the γ-ray transitions assigned to band 5.

Band 5							
E_γ (keV) [a]	I_γ [b]	A_2	A_4	δ	R	Mult.	Assignment
286.5	60	0.309(99)	0.135(120)	0.37(1)	1.07(2)	$M1/E2$	$(9^-\rightarrow 8^-)$
315.3	31.7	0.116(87)	−0.037(81)	0.22(5)	1.23(3)	$M1/E2$	$(10^-\rightarrow 9^-)$
329.8	1.5						$(17^-\rightarrow 16^-)$
340.0	16.6				1.20(4)	$M1/E2$	$(11^-\rightarrow 10^-)$
341.2	1.5						$(16^-\rightarrow 15^-)$
360.5	11.5				0.94(5)	$M1/E2$	$(12^-\rightarrow 11^-)$
369.3	2.6						$(15^-\rightarrow 14^-)$
375.9	5.5						$(13^-\rightarrow 12^-)$
381.6	3.5						$(14^-\rightarrow 13^-)$
601.6	20.7				1.09(4)	$E2$	$(10^-\rightarrow 8^-)$
655.2	30.0				0.80(3)	$E2$	$(11^-\rightarrow 9^-)$
661.4	16.4				1.02(4)	$E2$	$(18^-\rightarrow 16^-)$
670.7	16.2				1.07(3)	$E2$	$(17^-\rightarrow 15^-)$
700.3	34.8				1.00(4)	$E2$	$(12^-\rightarrow 10^-)$
702.5	10.3				1.15(9)	$E2$	$(19^-\rightarrow 17^-)$
710.1	26.2				1.07(3)	$E2$	$(16^-\rightarrow 14^-)$
736.3	31.2				1.07(4)	$E2$	$(13^-\rightarrow 11^-)$
751.4	22.2				1.08(3)	$E2$	$(15^-\rightarrow 13^-)$
757.4	33.4				1.08(5)	$E2$	$(14^-\rightarrow 12^-)$
772.1	8.7						$(20^-\rightarrow 18^-)$
836.7	9.0						$(21^-\rightarrow 19^-)$
904.4	9.3						$(22^-\rightarrow 20^-)$
976.2	5.3						$(23^-\rightarrow 21^-)$
1041.5	4.8						$(24^-\rightarrow 22^-)$
1109.3	3.5						$(25^-\rightarrow 23^-)$
1168.6	2.6						$(26^-\rightarrow 24^-)$
1266.8	0.9						$(28^-\rightarrow 26^-)$

[a]The γ-ray energies are estimated to be accurate to ± 0.3 keV for the strong transitions ($I_\gamma > 10$), rising to ± 0.6 keV for the weaker transitions.

[b]Errors on the relative intensities are estimated to be less than 5% of the quoted values for strong transitions ($I_\gamma > 10$) and less than 10% for the weaker transitions.

states, the dominant components of which are included in Table VII for each level.

C. Alignment and energy systematics

The experimental data are presented in Fig. 11 in terms of an alignment i_x plot [52], as a function of rotational frequency, $\omega \approx E_\gamma/2\hbar$ for $\Delta I = 2$ transitions. A rotational reference, based on a configuration with a variable moment of inertia $\mathcal{J}_{ref} = \mathcal{J}_0 + \omega^2 \mathcal{J}_1$, with Harris parameters [53] $\mathcal{J}_0 = 22.7\hbar^2$ MeV^{-1} and $\mathcal{J}_1 = 16.6\hbar^4$ MeV^{-3}, has been subtracted in each case; band 3 over the frequency range $0.10 \leqslant \omega \leqslant 0.50$ MeV/$\hbar$ was used as the reference for this systematic comparison.

The energies of the linked bands 1–4 are shown, relative to a rigid-rotor reference, as a function of spin in Fig. 12. It can be seen that band 3 represents the yrast band at low spin but that band 1 becomes yrast at high spin.

D. Electromagnetic transition strengths

The determination of absolute $B(M1)$ and $B(E2)$ values requires the measurement of nuclear lifetimes. However, $B(M1)/B(E2)$ ratios of reduced transition probabilities may be readily extracted from experimental γ-ray branching ratios λ of competing $\Delta I = 2$ and $\Delta I = 1$ transitions, i.e.,

$$\frac{B(M1; I \rightarrow I-1)}{B(E2; I \rightarrow I-2)} = 0.697 \frac{[E_\gamma(I \rightarrow I-2)]^5}{[E_\gamma(I \rightarrow I-1)]^3} \times \frac{1}{\lambda} \frac{1}{[1+\delta^2]} \left[\frac{\mu_N^2}{e^2 b^2}\right], \quad (4)$$

with $\lambda = T_\gamma(I \rightarrow I-2)/T_\gamma(I \rightarrow I-1)$ and E_γ measured in MeV. Such ratios of reduced transition probabilities have been extracted for the strongly coupled bands 2–5 in ^{124}La and are shown in Fig. 13. The experimental $E2/M1$ multipole mixing ratios δ, where available, were used in calculat-

TABLE VI. Measured properties of the interband γ-ray transitions.

Bands	E_γ (keV) [a]	I_γ [b]	A_2	A_4	δ	R	Mult.	Assignment
$1\rightarrow 2a$	85.4	10.0						$(7^-\rightarrow 6^-)$
$2a\rightarrow 1$	127.6	34.1				0.60(3)	$M1/E2$	$(8^-\rightarrow 7^-)$
$1\rightarrow 2a$	171.0	53.8				0.54(2)	$M1/E2$	$(9^-\rightarrow 8^-)$
$1\rightarrow 2a$	207.5	5.3				0.60(3)	$M1/E2$	$(11^-\rightarrow 10^-)$
$2a\rightarrow 1$	215.9	26.0				0.56(3)	$M1/E2$	$(10^-\rightarrow 9^-)$
$1\rightarrow 2b$	401.6	22.9				0.71(3)	$E2$	$(11^-\rightarrow 9^-)$
$2b\rightarrow 3b$	591.3	5.6				0.69(6)	$E1$	$(11^-\rightarrow 10^+)$
$2a\rightarrow 3a$	636.4	10.4				0.50(9)	$E1$	$(12^-\rightarrow 11^+)$
$2b\rightarrow 3b$	759.6	9.6				0.64(8)	$E1$	$(13^-\rightarrow 12^+)$
$2a\rightarrow 3a$	767.1	9.4				0.69(6)	$E1$	$(14^-\rightarrow 13^+)$
$4a\rightarrow 3a$	840.9	26.9	0.194(100)	0.108(110)	0.28(10)	0.52(1)	$M1/E2$	$(12^+\rightarrow 11^+)$
$2a\rightarrow 3a$	845.4	7.5				0.51(3)	$M1/E2$	$(16^-\rightarrow 15^+)$
$2b\rightarrow 3b$	867.3	8.0						$(15^-\rightarrow 14^+)$
$4a\rightarrow 3a$	897.3	11.8						$(14^+\rightarrow 13^+)$
$4a\rightarrow 3a$	905.3	7.0						$(16^+\rightarrow 15^+)$
$4b\rightarrow 3b$	966.6	21.5	$-0.089(54)$	$\equiv 0$			$M1/E2$	$(13^+\rightarrow 12^+)$
$4b\rightarrow 3b$	978.0	9.1						$(15^+\rightarrow 14^+)$
$4a\rightarrow 3b$	1068.4	4.7						$(12^+\rightarrow 10^+)$
$4b\rightarrow 3a$	1174.0	5.4						$(13^+\rightarrow 11^+)$
$4a\rightarrow 3b$	1217.4	6.8						$(14^+\rightarrow 12^+)$
$4b\rightarrow 3a$	1257.5	3.1						$(15^+\rightarrow 13^+)$
$4a\rightarrow 3b$	1302.5	4.0						$(16^+\rightarrow 14^+)$
$4a\rightarrow 3b$	1349.5	2.5						$(18^+\rightarrow 16^+)$

[a]The γ-ray energies are estimated to be accurate to ± 0.3 keV for the strong transitions ($I_\gamma > 10$), rising to ± 0.6 keV for the weaker transitions.

[b]Errors on the relative intensities are estimated to be less than 5% of the quoted values for strong transitions ($I_\gamma > 10$) and less than 10% for the weaker transitions.

ing the $B(M1)/B(E2)$ ratios; otherwise, δ was set to zero (the ratios, $\propto [1+\delta^2]^{-1}$, are insensitive to the exact value of δ). In the framework of the rotational model, the expressions [54]

$$B(M1;I\rightarrow I-1)=\frac{3}{4\pi}\mu_N^2 G_{KK}^2 \langle IK10|I-1K\rangle^2,$$

$$B(E2;I\rightarrow I-2)=\frac{5}{16\pi}e^2 Q_0^2 \langle IK20|I-2K\rangle^2 \qquad (5)$$

can be combined to yield a theoretical ratio

$$\frac{B(M1;I\rightarrow I-1)}{B(E2;I\rightarrow I-2)}=\frac{8}{5}\frac{G_{KK}^2}{Q_0^2}\frac{(2I-1)}{(I-1+K)}\times\frac{(I-1)}{(I-1-K)}\left[\frac{\mu_N^2}{e^2b^2}\right]. \qquad (6)$$

The parameter G_{KK} is defined as

$$G_{KK}=K(g_K-g_R)=\Omega_p(g_{\Omega_p}-g_R)+\Omega_n(g_{\Omega_n}-g_R), \quad (7)$$

where g_K is the effective g factor of the related two-quasiparticle configuration and the g_Ω values are taken from Table VII. The rotational g factor g_R is taken as equal to $Z/A=0.460$ and $K=|\Omega_\pi \pm \Omega_\nu|$, coupled in accordance with the Gallagher-Moszkowski rules that require parallel intrinsic spins [55]. The quadrupole moment Q_0 can be estimated from the TRS-predicted deformation parameters (β_2, β_4, γ). Calculated $B(M1)/B(E2)$ ratios are included in Fig. 13.

Finally, the δ values were used to determine the ratio of $\Delta I=1$ to $\Delta I=2$ reduced $E2$ transition probabilities depopulating a level of spin I, i.e.,

$$\frac{B(E2;I\rightarrow I-1)}{B(E2;I\rightarrow I-2)}=\left[\frac{E_\gamma(I\rightarrow I-2)}{[E_\gamma(I\rightarrow I-1)}\right]^5\times\frac{1}{\lambda}\frac{\delta^2}{[1+\delta^2]}. \qquad (8)$$

Results for band 3 are shown in Fig. 14.

E. Configuration assignments

Based on previous work, experimental properties, and comparison to the Woods-Saxon cranking calculations, it has been possible to assign quasiparticle configurations to the bands in ^{124}La. The results are summarized in Table VIII and the band properties discussed below.

1. Bands 3 and 4: $\pi h_{11/2}\otimes\nu h_{11/2}$ bands

The flat i_x of band 3 for $\omega<0.5$ MeV/$\hbar$, shown in Fig. 11, implies a $\pi h_{11/2}\otimes\nu h_{11/2}$ configuration through blocking arguments; i.e., neither the theoretical ω_{EF} nor the ω_{ef} alignments of Fig. 10 are evident. In terms of the quasiparticle labels of Table VIII, the two signature components of band 3

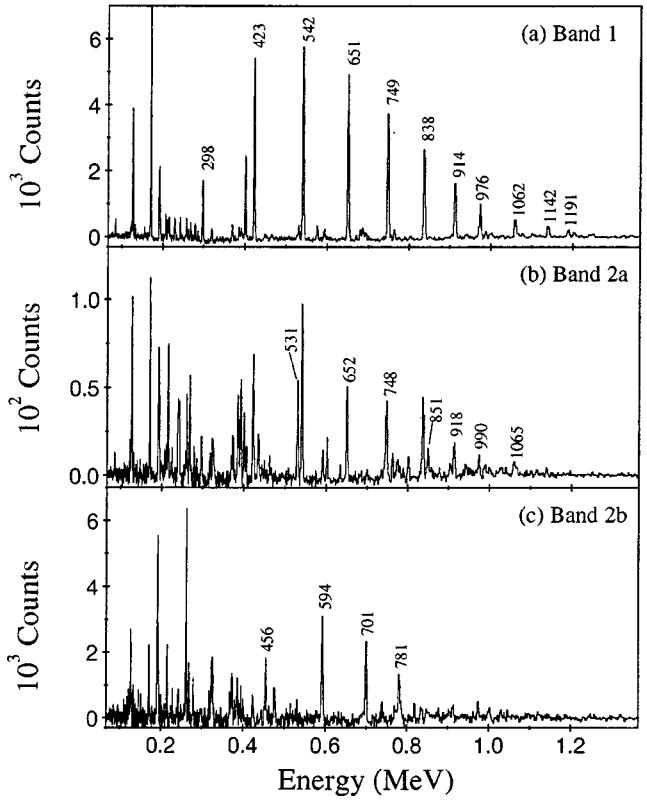

FIG. 4. Examples of background-subtracted γ-ray spectra showing transitions, labeled in keV, in bands 1 and 2 of ^{124}La.

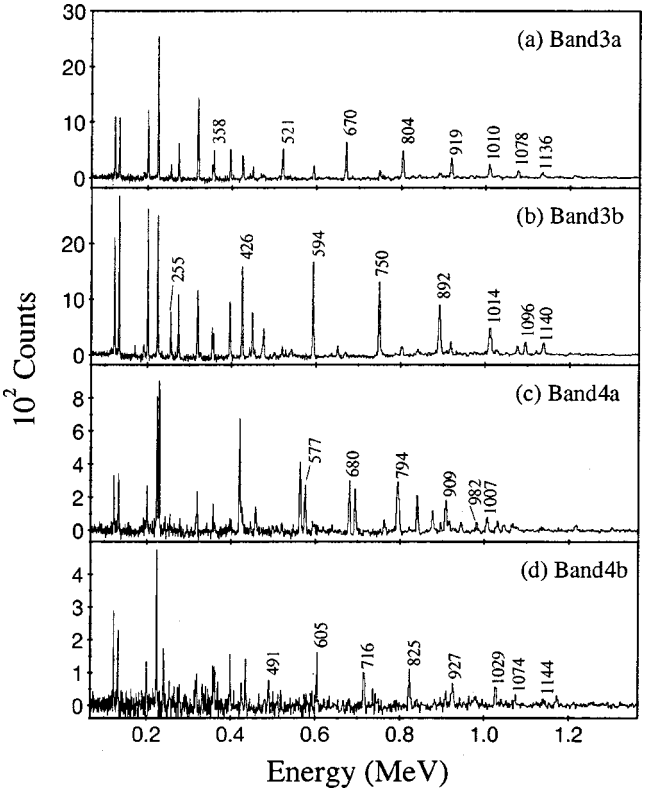

FIG. 5. Examples of background-subtracted γ-ray spectra showing transitions, labeled in keV, in bands 3 and 4 of ^{124}La.

correspond to Ee ($\alpha=1$) and Ef ($\alpha=0$) configurations, respectively. Similar to band 3, the proton ω_{EF} and neutron ω_{ef} alignments of Fig. 10 are absent (blocked) in band 4 and hence this band is assigned an excited $\pi h_{11/2}\otimes\nu h_{11/2}$ structure; the two signature components correspond to Fe ($\alpha=0$) and Ff ($\alpha=1$) configurations, respectively.

Both bands 3 and 4 show evidence for the rotational alignment of $h_{11/2}$ protons at $\omega\approx 0.50$ MeV/$\hbar$, corresponding to the ω_{FG} (band 3) and ω_{EH} (band 4) alignments in Fig. 10(a). The rigid-rotor plots for bands 3 and 4 (Fig. 12) show that the energy splitting between the bands decreases with increasing spin, and at $I\sim 26\hbar$ after a backbend, the excited band becomes energetically favored. The signature splitting within the two bands is related to the energy splitting of the $\nu h_{11/2}$ orbital, while the energy difference between the two bands is related to the energy splitting of the $\pi h_{11/2}$ orbital. However, the latter splitting of the E and F orbitals is expected to increase with spin, as shown in Fig. 10(a). A similar situation is seen in the corresponding twin $\pi h_{11/2}\otimes\nu h_{11/2}$ bands of ^{134}Pr and has been attributed to different quadrupole deformations [56] and more recently to chiral symmetry [10].

The favored signature component of a specific j shell is given by $\alpha_f=j \bmod 2$. Moreover, the favored signature component of a specific $j_\pi\otimes j_\nu$ shell-model configuration in a doubly odd nucleus is expected to be

$$\alpha_f=[j_\pi+j_\nu]\bmod 2. \tag{9}$$

For example, the favored signature component of the yrast $\pi h_{11/2}\otimes\nu h_{11/2}$ configuration should have $\alpha_f=[11/2+11/2]\bmod 2=1$, or odd spins. However, with this definition, band 3 exhibits a signature inversion at low spin with the ''favored'' odd-spin component actually higher in energy than the ''unfavored'' even-spin component. The signatures invert at $I_c=(18.5\hbar)$, corresponding to a rotational frequency $\omega=0.45$ MeV/$\hbar$; this is evident in Fig. 15 which plots the staggering parameter [57], defined as

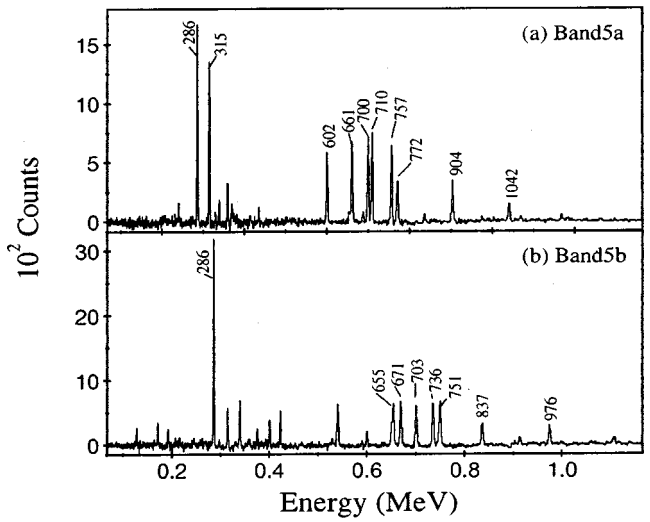

FIG. 6. Examples of background-subtracted γ-ray spectra showing transitions, labeled in keV, in band 5 of ^{124}La.

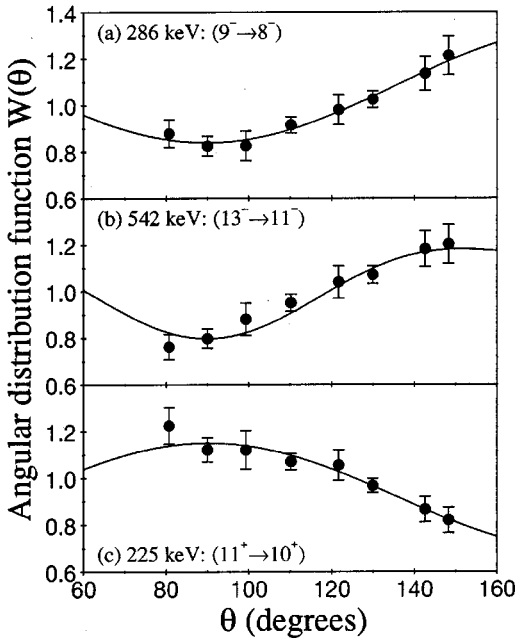

FIG. 7. Examples of angular distributions. Experimental intensities are shown by the data points, while fitted angular-distribution functions are shown by the curves. The 286-keV transition (a) is a $\Delta I=1$ transition of band 5 with $\delta>0$; the 542-keV transition (b) is a $\Delta I=2$ transition of band 1; the 225-keV transition (c) is a $\Delta I=1$ transition of band 3.

$$S(I)=E(I)-E(I-1)-\tfrac{1}{2}[E(I+1)-E(I)+E(I-1)-E(I-2)], \quad (10)$$

as a function of spin. In band 3, the splitting is related to the energy difference of the two signatures of the $\nu h_{11/2}$ orbital [levels e and f in Fig. 10(b)]. It should be noted that the e and f orbitals are essentially degenerate at low spin and frequency and no signature splitting should occur in band 3 at low spin. The corresponding $\pi h_{11/2}\otimes\nu h_{11/2}$ bands in odd-odd ^{122}La [58] and ^{126}La [46,59] are also included in Fig. 15(b), taking spin assignments from smooth systematic trends as proposed by Ref. [8]. It can be seen that the inversion spin systematically increases with mass number as noted in Ref. [2] for odd-odd caesium and lanthanum isotopes.

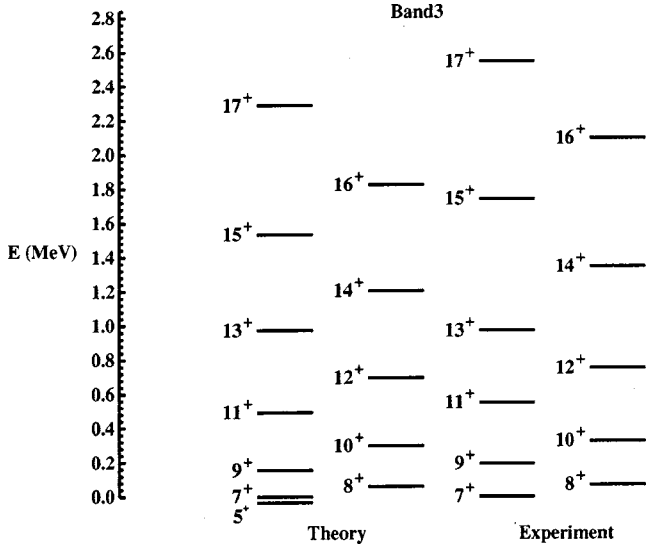

FIG. 8. Comparison of the energy levels of band 3 in ^{124}La with results of the CQPCM for the first $\pi h_{11/2}\otimes\nu h_{11/2}$ configuration. Theory suggests a spin of $7\hbar$ for the lowest experimental state of band 3.

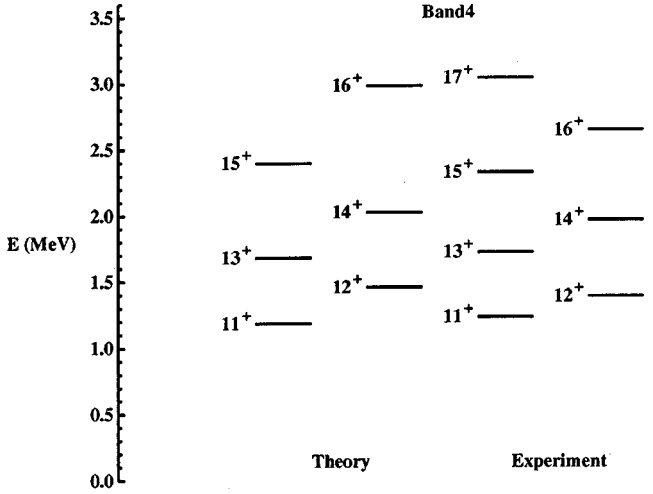

FIG. 9. Comparison of the energy levels of band 4 in ^{124}La with results of the CQPCM for the second $\pi h_{11/2}\otimes\nu h_{11/2}$ configuration.

In the case of band 4 [Fig. 15(c)], there is a large signature splitting at low spin. For the excited $\pi h_{11/2}\otimes\nu h_{11/2}$ con-

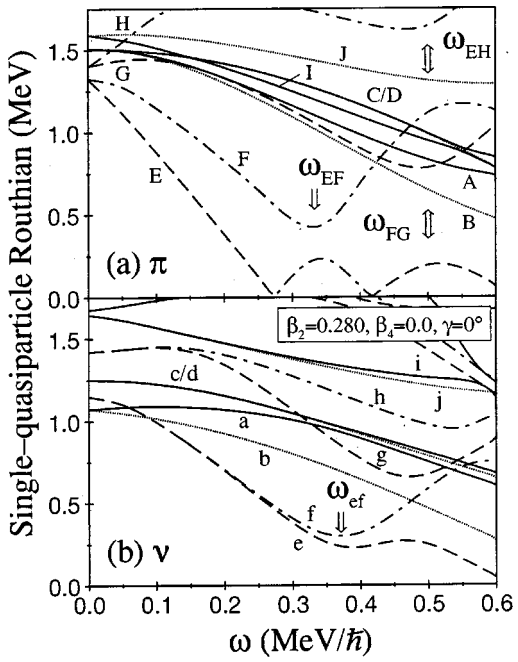

FIG. 10. Representative cranked Woods-Saxon single-quasiparticle energies, appropriate for ^{124}La, for protons (a) and neutrons (b). The parity and signature (π,α) of the levels are (+, +1/2), solid lines; (+,−1/2), dotted lines; (−,−1/2), dashed lines; (−,+1/2), dot-dashed lines. Quasiparticle alignments are indicated by the arrows and labeled by the aligning quasiparticles.

TABLE VII. Quasiparticle orbitals as labeled in Fig. 10 with their dominant Nilsson components and calculated g factors. The calculations were performed with $\beta_2=0.28$ and $\gamma=0°$.

	Label		Nilsson configuration		g factor
	$\alpha=+1/2$	$\alpha=-1/2$	$[Nn_z\Lambda]\Omega^\pi$	Subshell	g_Ω
π	A	B	$[422]3/2^+$ (91%)	$g_{7/2}$	0.54
	C	D	$[404]9/2^+$ (93%)	$g_{9/2}$	1.32
	F	E	$[550]1/2^-$ (89%)	$h_{11/2}$	1.65
	H	G	$[541]3/2^-$ (90%)	$h_{11/2}$	1.50
	I	J	$[420]1/2^+$ (80%)	$d_{5/2}$	2.52
ν	a	b	$[411]1/2^+$ (77%)	$d_{3/2}$	1.85
	c	d	$[413]5/2^+$ (92%)	$g_{7/2}$	0.38
	f	e	$[523]7/2^-$ (90%)	$h_{11/2}$	−0.32
	h	g	$[532]5/2^-$ (88%)	$h_{11/2}$	−0.38
	i	j	$[402]5/2^+$ (75%)	$d_{5/2}$	−0.48

figuration, the proton F orbital ($\alpha=1/2$) is coupled to the neutron e and f orbitals and the favored signature Fe has $\alpha=0$, or even spins. This is indeed the case for band 4 at low spin, but there is now a signature inversion *above* I_c in band 4 in contrast to the signature inversion *below* I_c in band 3. Moreover, the signatures cross again in band 4 at $I=(24.5\hbar)$, but this could be related to perturbations of the smooth band behavior by alignments of quasiparticle pairs. Indeed, there is a sharp backbend in the $\alpha=1$ signature of band 4 rather than a more gradual upbend as seen in the $\alpha=0$ signature and both signatures of band 3 at $\omega\approx0.5$ MeV/$\hbar$, as evident in Fig. 11(b).

The behavior of the signatures in bands 3 and 4 of ^{124}La is consistent with the ''signature quartette'' description of

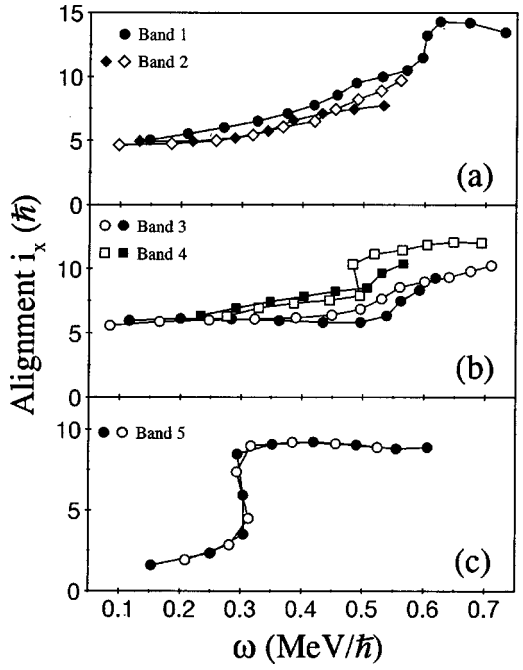

FIG. 11. Experimental alignment plots for the bands in ^{124}La.

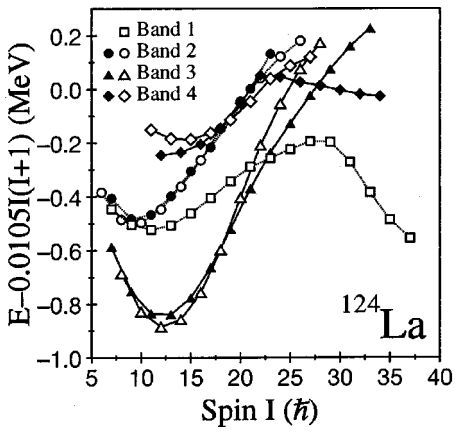

FIG. 12. Experimental rigid-rotor plots for bands 1–4.

Ref. [60]; the excited $\pi h_{11/2}\otimes\nu h_{11/2}$ band is predicted to show signature inversion *above* the critical spin. The behavior of the two $\pi h_{11/2}\otimes\nu h_{11/2}$ bands in ^{124}La is also similar to the chiral-partner bands seen in this mass region [10,61,62], where low-spin signature inversion is seen in one (the yrast configuration), but not both, chiral partners of the $\pi h_{11/2}\otimes\nu h_{11/2}$ configuration. Furthermore, it has been suggested that signature inversion and chirality may be intimately related [63].

The experimental $B(M1;I\to I-1)/B(E2;I\to I-2)$ ratios for band 3 also show a clear signature dependence, as can be seen in Fig. 13(b). The ratios are larger for the transitions from the $\alpha=1$ signature to the $\alpha=0$ signature compared to those for the transitions from the $\alpha=0$ signature to

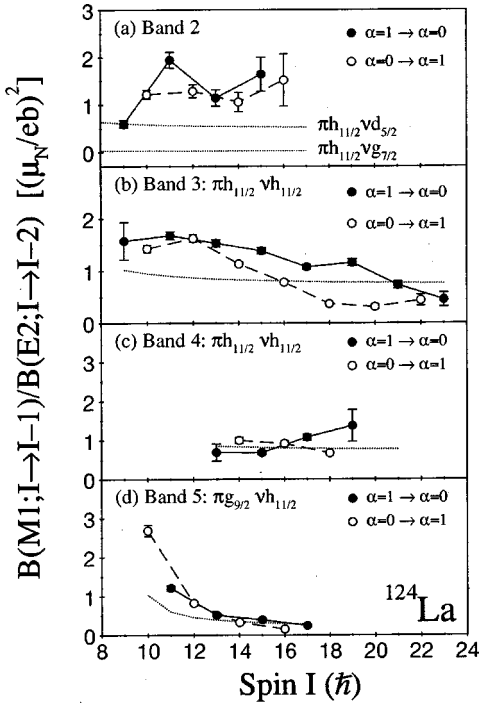

FIG. 13. Experimental $B(M1;I\to I-1)/B(E2;I\to I-2)$ ratios of reduced transition probabilities for the $\Delta I=1$ bands in ^{124}La. The dotted lines show theoretical estimates obtained for the given configurations.

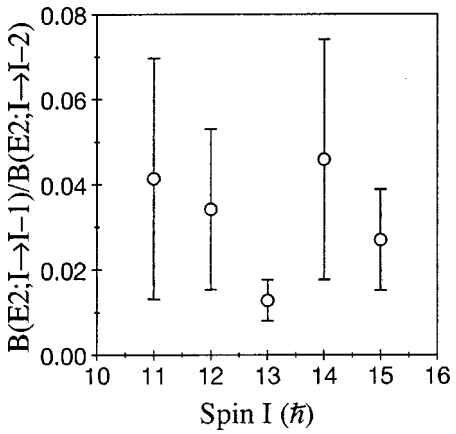

FIG. 14. Experimental $B(E2;I\rightarrow I-1)/B(E2;I\rightarrow I-2)$ ratios of reduced transition probabilities for band 3 in ^{124}La.

the $\alpha=1$ signature; unlike the level energies, no signature inversion is evident, which is, however, consistent with neighboring odd-odd nuclei [15,34]. Calculated $B(M1)/B(E2)$ ratios for the $\pi h_{11/2}\otimes\nu h_{11/2}$ configuration are included in Figs. 13(b) and 13(c) and on average agree with the experimental values. The experimental $B(E2;I\rightarrow I-1)/B(E2;I\rightarrow I-2)$ ratios for band 3, shown in Fig. 14, could not be determined with sufficient sensitivity to examine signature effects, but have an average value of approximately 0.03. Any signature dependence (staggering) in the $B(M1;I\rightarrow I-1)/B(E2;I\rightarrow I-2)$ or $B(E2;I\rightarrow I-1)/B(E2;I\rightarrow I-2)$ ratios must be attributed to the $\Delta I=1$ reduced transition probabilities rather than the $B(E2;I\rightarrow I-2)$ values; neither experimental nor theoretical evidence exists which suggests that the latter quantities should exhibit significant signature-dependent effects. The signature effect of the $M1$ transition probabilities is entirely due to the Coriolis mixing of $\Omega=1/2$ states in the nuclear wave function and can occur for axially symmetric or triaxial shapes. However, a significant signature dependence of the nonstretched $E2$ transition probabilities only occurs for nonaxial shapes [64].

In the literature, signature inversion has been attributed to a triaxial nuclear shape with $\gamma>0°$, Lund convention [65], in conjunction with the specific position of the Fermi surface within a given subshell [66]. Positive γ corresponds to rotation about the short axis of the triaxial nuclear shape. In the present case of ^{124}La, cranked shell-model calculations indicate a signature inversion for the $\nu h_{11/2}$ orbital for γ only slightly positive; results calculated at a rotational frequency $\omega=0.25$ MeV/$\hbar$ are shown in Fig. 16, where the inversion of the e and f orbitals can be seen at $\gamma>4°$. For higher frequencies, the inversion point increases slightly such that it has reached $\gamma=10°$ at $\omega=0.50$ MeV/$\hbar$. The signature inversion in band 3 of ^{124}La could thus be simply explained by

TABLE VIII. Quasiparticle assignments to the rotational bands in ^{124}La at low spin.

Band	Quasiparticle label	Dominant configuration
1	Eb	$\pi h_{11/2}\otimes\nu d_{3/2}$
2	Ei, Ej [a]	$\pi h_{11/2}\otimes\nu d_{5/2}$
3	Ee, Ef	$\pi h_{11/2}\otimes\nu h_{11/2}$
4	Fe, Ff	$\pi h_{11/2}\otimes\nu h_{11/2}$
5	Ce, De	$\pi g_{9/2}\otimes\nu h_{11/2}$

[a]Preferred assignment based on electromagnetic properties.

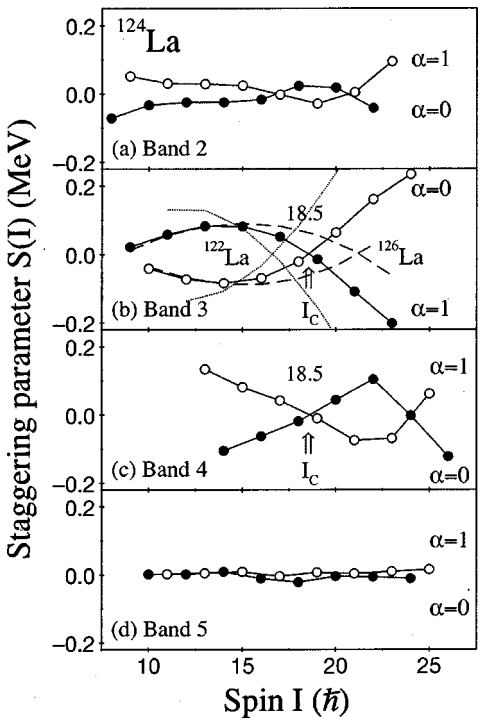

FIG. 15. Plot of the energy staggering parameter $S(I)$ versus assumed spin I for the $\Delta I=1$ bands in ^{124}La. The solid and open symbols represent the two signatures of each band, with the solid symbol corresponding to the theoretically "favored" component. In (b) the dotted and dashed lines represent the corresponding bands in ^{122}La and ^{126}La, respectively.

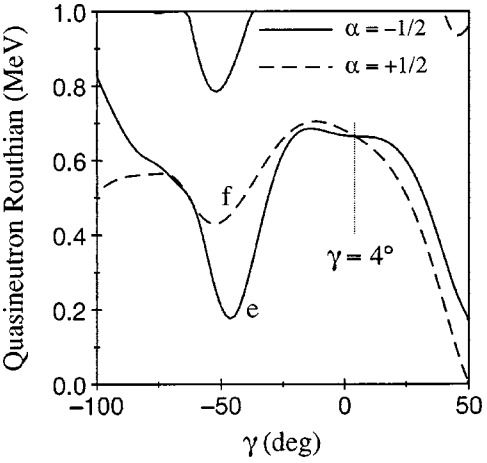

FIG. 16. Quasineutron levels calculated as a function of the triaxiality parameter γ for ^{124}La at a rotational frequency $\omega=0.25$ MeV/$\hbar$. An inversion of the e and f levels, derived from a $\nu h_{11/2}$ orbital, can be seen at $\gamma=4°$, which is close to the axial prolate shape with $\gamma=0°$.

small positive γ deformation ($\gamma \gtrsim 4°$) for spins $I < I_c$ and an axially symmetric shape ($\gamma \approx 0°$) for $I > I_c$. However, the *opposite* effect would be needed to explain the high-spin signature inversion of band 4, i.e., $\gamma \approx 0°$ for $I < I_c$ and $\gamma \gtrsim 4°$ for $I > I_c$. This unlikely scenario suggest that signature inversion is related to other physical effects.

Signature inversion is only ever seen in multiquasiparticle configurations and has been attributed to a residual proton-neutron (p-n) interaction [15]. In the case of a semide-coupled [37] structure, such as band 3, low-spin signature inversion has been attributed to a large repulsive matrix element of the p-n force acting in the maximally aligned intrinsic state [3]. In the present case, this state with $I_{max} = 11\hbar$ is pushed up in energy and the system behaves effectively with $I_{max} = 10\hbar$ and has a favored even-spin sequence. With increasing rotation, however, the $I_{max} = 11\hbar$ state becomes more favored such that the signature branches cross at the inversion spin I_c.

More recently, quadrupole pairing correlations have been considered. "Extended TRS" calculations [45], which include a quadrupole pairing force, suggest that the $(\lambda\mu) = (22)$ component is dominant in inducing signature inversion in $A \sim 125$ nuclei around the $\nu h_{11/2}$ midshell, i.e., nuclei with $N = 65$, 67, prime examples being ^{122}La and ^{124}La. These calculations predict a triaxial shape with $\beta_2 \approx 0.29$ and $\gamma \approx +13°$ for the $\pi h_{11/2} \otimes \nu h_{11/2}$ configuration in ^{124}La. In contrast, the simpler TRS calculations used here yield an axially symmetric shape with $\beta_2 = 0.28$ and $\gamma = 0°$ while the CQCPM calculations also yield $\gamma \approx 13°$.

A test of triaxiality has been proposed in Ref. [67] that is related to measured $B(M1)$ rates between favored and unfavored signature components of a rotational band. Taking a unique-parity high-spin orbital (e.g., $h_{11/2}$) in an odd-A nucleus, the following relation was shown to be valid for axially symmetric shapes:

$$\frac{\Delta B(M1)}{\langle B(M1)\rangle} = \frac{4(\Delta e'/\hbar\omega)}{1+(\Delta e'/\hbar\omega)^2}. \tag{11}$$

Here $\Delta B(M1) = B(M1; I \to I-1) - B(M1; I-1 \to I-2)$ is the difference in the $B(M1)$ rates for $\Delta I = 1$ transitions from one signature to the other and vice versa, while $\langle B(M1)\rangle$ is the average value. The quantity $\Delta e'/\hbar\omega$ is the ratio of the experimental signature splitting of the Routhians [52] divided by the rotational frequency. The definition of spin ensures that $\Delta e' = 0$ at the inversion spin $I_c = (18.5\hbar)$. Comparison of the left-hand side of Eq. (11) to the right-hand side yields a test for triaxiality. Assuming a constant rotational stretched $B(E2)$ rate, the $B(M1)$ values of Eq. (11) may be substituted by the measured $B(M1)/B(E2)$ ratios (Fig. 13). If Eq. (11) can be generalized to the case of two unique-parity orbitals in an odd-odd nucleus (e.g., the $\pi h_{11/2} \otimes \nu h_{11/2}$ configuration), it immediately implies that there should be no signature dependence in the $B(M1)$ rates when $\Delta e' = 0$, i.e., $\Delta B(M1) \to 0$ around the signature inversion spin $I_c = (18.5\hbar)$. Results for band 3 are plotted in Fig. 17, where it can be seen that a constant difference in the ratios is observed for spins below $20\hbar$. However, at $I \approx 22\hbar$, which is just above the signature-inversion spin, the ratios become approximately equal. This behavior could be interpreted as a shape change from triaxial ($\gamma > 0°$) to axially symmetric ($\gamma = 0°$) around the inversion spin.

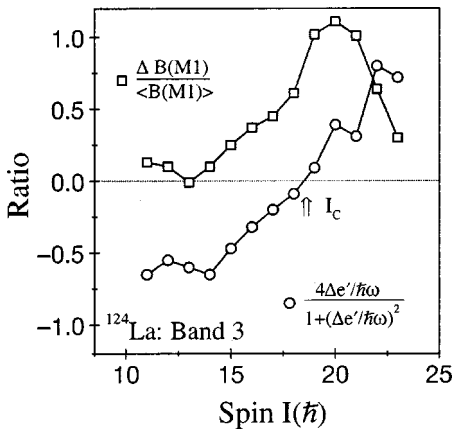

FIG. 17. These ratios plotted for band 3 as a function of spin should be equal for an axially symmetric shape, as discussed in the text.

2. Band 1: $\pi h_{11/2} \otimes \nu d_{3/2}$ band

The decoupled nature of band 1 implies that it is built on a configuration with a low K value. It is hence assigned a $K^\pi = 0^-, 1^-$ $\pi h_{11/2} \otimes \nu d_{3/2}$ doubly decoupled [38] configuration making use of the $\Omega = 1/2$ E and b orbitals (see Fig. 10 and Table VII). A similar band is seen in the ^{126}La isotope [46] and a decoupled band has also been observed in the ^{126}Pr isotone [68], with possibly the same configuration, although a positive-parity $\pi h_{11/2} \otimes \nu h_{9/2}$ structure was also considered.

Band 1 shows evidence for a rotational alignment of particles at $\omega \approx 0.60$ MeV/$\hbar$. This is most likely the ω_{ef} alignment of $h_{11/2}$ neutrons in Fig. 10, which is blocked in all other bands. Experimentally, the alignment occurs much later than expected: $\omega_{ef} \approx 0.36$ MeV/$\hbar$ in Fig. 10(b). Furthermore, the alignment frequency in ^{124}La is even higher than the corresponding neutron alignments in the $\pi h_{11/2}$ bands of neighboring odd-A lanthanum isotopes, which occur at 0.45–0.50 MeV/$\hbar$ [18]. The discrepancy between predicted and experimental $\nu h_{11/2}$ alignment frequencies is a common feature of this mass region and has been discussed in detail in Refs. [18,69]; proton-neutron pairing or deformation effects have been considered as an explanation of the discrepancy.

3. Band 2: $\pi h_{11/2} \otimes \nu d_{5/2}$ band

Band 2 is formed by coupling the $\pi h_{11/2}$ intruder orbital to higher-lying positive parity neutron orbitals. The theoretical results of Fig. 10 and Table VII show two possible $\Omega^\pi = 5/2^+$ orbitals based on $\nu[413]5/2^+$ ($g_{7/2}$, with near-degenerate signature components c and d) and $\nu[402]5/2^+$ ($d_{5/2}$, with components i and j), respectively. These calculations, performed with $\beta_2 = 0.28$ and $\gamma = 0°$, suggest that the $K^\pi = 3^-$ $\pi h_{11/2} \otimes \nu g_{7/2}$ configuration, with signature compo-

nents Ec ($\alpha=0$) and Ed ($\alpha=1$), would be energetically favored over the $K^{\pi}=3^{-}$ $\pi h_{11/2}\otimes\nu d_{5/2}$ configuration, with signature components Ei ($\alpha=0$) and Ej ($\alpha=1$). However, the $B(M1)/B(E2)$ ratios for band 2 are more consistent with estimations for the latter configuration; the $l+1/2$ $\nu d_{5/2}$ orbital induces larger $B(M1)$ values than the $l-1/2$ $\nu g_{7/2}$ orbital. Hence the $\pi h_{11/2}\otimes\nu d_{5/2}$ configuration is the preferred assignment for band 2. With this assignment the correct signature ($\alpha=0$) is favored at low spin in Fig. 15(a). The signatures do cross, however, for spins around $18.5\hbar$ which is the inversion spin for bands 3 and 4 [Figs. 15(b) and 15(c), respectively].

The $\pi h_{11/2}\otimes\nu d_{5/2}$ configuration has also been assigned to the corresponding band in ^{126}La [46]. The present cranking calculations can be reconciled with this configuration by changing the quadrupole deformation parameters. While a decrease in β_2 slightly lowers the excitation energy of the i and j levels ($\nu d_{5/2}$) in Fig. 10(b), a more dramatic change occurs when introducing triaxiality with $\gamma>0°$. Indeed, for $\gamma\approx 20°$ the c/d ($\nu g_{7/2}$) and i/j ($\nu d_{5/2}$) levels all become degenerate at zero frequency. It should be noted that triaxiality with positive γ also inverts the signatures of the yrast $\pi h_{11/2}\otimes\nu h_{11/2}$ band, as discussed previously in Sec. IV E 1.

4. Band 5: $\pi g_{9/2}\otimes\nu h_{11/2}$ band

The $\Delta I=1$ transitions of band 5 have angular distributions with positive A_2 coefficients (Table V), implying $\delta>0$. Such unusual behavior is characteristic of the $\pi g_{9/2}$ orbital which originates below the spherical $Z=50$ gap. Indeed, $\Delta I=1$ transitions with positive multipole mixing ratios have systematically been observed in $\pi g_{9/2}\otimes\nu h_{11/2}$ bands in doubly odd antimony ($Z=51$) [12] and iodine ($Z=53$) [13] isotopes. Hence, band 5 in ^{124}La is assigned a similar $\pi g_{9/2}\otimes\nu h_{11/2}$ configuration with degenerate signature components Ce ($\alpha=0$) and De ($\alpha=1$). Such a configuration has $K^{\pi}=8^{-}$ and is based on the $\pi[404]9/2^{+}\otimes\nu[523]7/2^{-}$ configuration, leading to the spin assignments of Fig. 3. The sign of the mixing ratio is related to the sign of the quantity (g_K-g_R) for a prolate nuclear shape. The value of (g_K-g_R) can be estimated from Eq. (7) and is indeed found to be positive for the assigned configuration of band 5.

The experimental $B(M1)/B(E2)$ ratios for band 5, shown in Fig. 13(d), are larger at low spin than for the other bands. The ratios decrease with increasing spin but, at the lowest spins, are larger than the predictions of the rotational model for the $\pi g_{9/2}\otimes\nu h_{11/2}$ configuration.

Unlike the other bands in ^{124}La, which all contain an $h_{11/2}$ proton which blocks the first allowed proton alignment, band 5 exhibits the ω_{EF} proton alignment of an $h_{11/2}$ pair. This alignment takes place at a frequency of $\omega\approx 0.30$ MeV/$\hbar$, close to the predicted frequency in Fig. 10(a). Similar alignments are seen in strongly coupled $\pi g_{9/2}$ bands of odd-A ^{121,123,125}La [16–18]. In Fig. 15(d), the two signatures of band 5 are degenerate below $I=14\hbar$. Above this spin, a small signature splitting is observed with the expected $\alpha=0$ component favored.

V. CONCLUSIONS

The doubly odd nucleus $^{124}_{57}La_{67}$ has been studied to high spin using the Gammasphere γ-ray spectrometer in conjunction with ancillary charged-particle and neutron detectors and the Argonne Fragment Mass Analyzer. The low-spin yrast band, based on a $\pi h_{11/2}\otimes\nu h_{11/2}$ configuration, exhibits a signature inversion in its level energies *below* $I_c=(18.5\hbar)$. A second band is also associated with an excited $\pi h_{11/2}\otimes\nu h_{11/2}$ configuration and shows a signature inversion *above* $I_c=(18.5\hbar)$. The yrast $\pi h_{11/2}\otimes\nu h_{11/2}$ band also exhibits a clear signature dependence (staggering) in its measured $B(M1)/B(E2)$ ratios of reduced transition probabilities, but with no change of phase (inversion) evident; the ratios are larger for transitions from the $\alpha=1$ signature to the $\alpha=0$ signature.

A third band is assigned a $\pi h_{11/2}\otimes\nu d_{5/2}$ configuration. A $\Delta I=2$ band, based on the $K^{\pi}=1^{-}$ $\pi h_{11/2}\otimes\nu d_{3/2}$ configuration, was also observed. Finally, a stongly coupled band, based on a high-K ($K^{\pi}=8^{-}$) $\pi g_{9/2}\otimes\nu h_{11/2}$ configuration was also established and is believed to be built on the ''high-spin'' isomer observed in previous β-decay studies. This band represents the first evidence for the $\pi g_{9/2}$ proton (hole) orbital in a doubly odd lanthanum isotope.

ACKNOWLEDGMENTS

This work was supported in part by the U.K. Engineering and Physical Sciences Research Council, U.S. National Science Foundation, and the Department of Energy, Nuclear Physics Division, under Contract No. W-31-109-ENG-38 (ANL). We are indebted to Dr. D. C. Radford for providing the RADWARE analysis codes and to Dr. R. Wyss and Dr. W. Nazarewicz for providing the Woods-Saxon cranking codes.

[1] A. J. Kreiner and M. A. J. Mariscotti, J. Phys. G **6**, L13 (1980).
[2] J. F. Smith, C. J. Chiara, D. B. Fossan, G. J. Lane, J. F. Lewicki, J. M. Sears, and P. Vaska, Phys. Rev. C **58**, 3237 (1998).
[3] M. A. Cardona *et al.*, Phys. Rev. C **59**, 1298 (1999).
[4] A. J. Kreiner and M. A. J. Mariscotti, Phys. Rev. Lett. **43**, 1150 (1979).
[5] R. Zheng, S. Zhu, N. Cheng, and J. Wen, Phys. Rev. C **64**, 014313 (2001), and references therein.
[6] Y. Liu, Y. Ma, H. Yang, and S. Zhou, Phys. Rev. C **52**, 2514 (1995).
[7] J. Timár *et al.*, Acta Phys. Pol. B **33**, 493 (2002).
[8] Y. Liu, J. Lu, Y. Ma, S. Zhou, and H. Zheng, Phys. Rev. C **54**, 719 (1996).
[9] S. Frauendorf and Jie Meng, Nucl. Phys. **A617**, 131 (1997).
[10] K. Starosta *et al.*, Phys. Rev. Lett. **86**, 971 (2001).
[11] N. Idrissi *et al.*, Z. Phys. A **341**, 427 (1992).
[12] S. Vajda, W. F. Piel, Jr., M. A. Quader, W. A. Watson III, F. C.

Yang, and D. B. Fossan, Phys. Rev. C **27**, 2995 (1983).
[13] M. A. Quader, W. F. Piel, Jr., S. Vajda, W. A. Watson III, F. C. Yang, and D. B. Fossan, Phys. Rev. C **30**, 1772 (1984).
[14] J. F. Smith *et al.* (unpublished).
[15] B. Cederwall *et al.*, Nucl. Phys. **A542**, 454 (1992).
[16] B. Cederwall, A. Johnson, B. Fant, S. Juutinen, P. Ahonen, S. Mitarai, J. Mukai, and J. Nyberg, Z. Phys. A **338**, 463 (1991).
[17] R. Wyss, F. Lidén, J. Nyberg, A. Johnson, D. J. G. Love, A. H. Nelson, D. W. Banes, J. Simpson, A. Kirwan, and R. Bengtsson, Nucl. Phys. **A503**, 244 (1989).
[18] D. J. Hartley, L. L. Riedinger, H. Q. Jin, W. Reviol, B. H. Smith, A. Galindo-Uribarri, D. G. Sarantites, D. R. LaFosse, J. N. Wilson, and S. M. Mullins, Phys. Rev. C **60**, 014308 (1999).
[19] A. Galindo-Uribarri *et al.*, Phys. Rev. C **50**, R2655 (1994).
[20] A. Galindo-Uribarri, S. M. Mullins, D. Ward, M. Cromaz, J. DeGraaf, T. E. Drake, S. Flibotte, V. P. Janzen, D. C. Radford, and I. Ragnarsson, Phys. Rev. C **54**, R454 (1994).
[21] T. B. Brown *et al.*, Phys. Rev. C **56**, R1210 (1997).
[22] D. J. Hartley *et al.*, Phys. Rev. C **55**, R985 (1997).
[23] F. G. Kondev *et al.*, Eur. Phys. J. A **2**, 249 (1998).
[24] F. G. Kondev *et al.*, Phys. Rev. C **59**, 3076 (1999).
[25] S. M. Mullins *et al.*, Phys. Rev. C **58**, R2626 (1998).
[26] A. V. Afanasjev and I. Ragnarsson, Nucl. Phys. **A608**, 176 (1996).
[27] I. Y. Lee, Nucl. Phys. **A520**, 641c (1990).
[28] D. G. Sarantites, P.-F. Hua, M. Devlin, L. G. Sobotka, J. Elson, J. T. Hood, D. R. LaFosse, J. E. Sarantites, and M. R. Maier, Nucl. Instrum. Methods Phys. Res. A **381**, 418 (1996).
[29] ''The Microball,'' URL: http://wunmr.wustl.edu/~dgs/mball/
[30] ''The Neutron Shell,'' URL: http://wunmr.wustl.edu/~dgs/NeutronShell/
[31] C. N. Davids, B. B. Back, K. Bindra, D. J. Henderson, W. Kutschera, T. Lauritsen, Y. Nagame, P. Sugathan, A. V. Ramayya, and W. B. Walters, Nucl. Instrum. Methods Phys. Res. B **70**, 358 (1992).
[32] C. E. Svensson *et al.*, Nucl. Instrum. Methods Phys. Res. A **396**, 228 (1997).
[33] D. C. Radford, Nucl. Instrum. Methods Phys. Res. A **361**, 297 (1995); **361**, 306 (1995).
[34] T. Komatsubara *et al.*, Nucl. Phys. **A557**, 419c (1993).
[35] T. Yamazaki, At. Data Nucl. Data Tables **A3**, 579 (1967).
[36] E. der Mateosian and A. W. Sunyar, At. Data Nucl. Data Tables **13**, 391 (1974).
[37] A. J. Kreiner, J. Davidson, M. Davidson, D. Abriola, C. Pomar, and P. Thieberger, Phys. Rev. C **36**, 2309 (1987).
[38] A. J. Kreiner, D. E. Di Gregorio, A. J. Fendrik, J. Davidson, and M. Davidson, Phys. Rev. C **29**, 1572 (1984).
[39] Ch. Droste, D. Chlebowska, J. Dobaczewski, F. Dönau, A. Kerek, G. Leander, J. Srebrny, and W. Waluś, Nucl. Phys. **A341**, 98 (1980), and references therein.
[40] F. Dönau and U. Hagemann, Z. Phys. A **293**, 31 (1979), and references therein.
[41] H. Dias and L. Losano, Phys. Rev. C **50**, 1377 (1994), and references therein.
[42] K. Starosta *et al.*, Phys. Rev. C **55**, 2794 (1997).
[43] T. Morek, K. Starosta, Ch. Droste, D. Fossan, G. Lane, J. Sears, J. Smith, and P. Vaska, Eur. Phys. J. A **3**, 99 (1998).
[44] K. Starosta, C. J. Chiara, D. B. Fossan, T. Koike, T. T. S. Kuo, D. R. LaFosse, S. G. Rohoziński, Ch. Droste, T. Morek, and J. Srebrny, Phys. Rev. C **65**, 044328 (2002).
[45] F. R. Xu, W. Satuła, and R. Wyss, Nucl. Phys. **A669**, 119 (2000).
[46] J. Timár *et al.*, Eur. Phys. J. A **7**, 7 (2000).
[47] W. Nazarewicz, J. Dudek, R. Bengtsson, and I. Ragnarsson, Nucl. Phys. **A435**, 397 (1985).
[48] S. Cwiok, J. Dudek, W. Nazarewicz, W. Skalski, and T. Werner, Comput. Phys. Commun. **46**, 379 (1987).
[49] R. Wyss, J. Nyberg, A. Johnson, R. Bengtsson, and W. Nazarewicz, Phys. Lett. B **215**, 211 (1988).
[50] W. Nazarewicz, G. A. Leander, and J. Dudek, Nucl. Phys. **A467**, 437 (1987).
[51] W. Nazarewicz, R. Wyss, and A. Johnson, Nucl. Phys. **A503**, 285 (1989).
[52] R. Bengtsson and S. Frauendorf, Nucl. Phys. **A327**, 139 (1979).
[53] S. M. Harris, Phys. Rev. **138**, B509 (1965).
[54] A. Bohr and B. R. Mottelson, *Nuclear Structure* (Benjamin, New York, 1975), p. 44.
[55] C. J. Gallagher, Jr. and S. A. Moszkowski, Phys. Rev. **111**, 1282 (1958).
[56] C. M. Petrache, D. Bazzacco, S. Lunardi, C. Rossi-Alvarez, G. De Angelis, M. De Poli, D. Bucurescu, C. A. Ur, P. B. Semmes, and R. Wyss, Nucl. Phys. **A597**, 106 (1996).
[57] A. J. Kreiner, M. A. J. Mariscotti, C. Baktash, E. der Mateosian, and P. Thieberger, Phys. Rev. C **23**, 748 (1981).
[58] D. R. LaFosse (private communication); Proceedings of the 2nd Biennial Workshop on Nuclear Structure Physics Near the Coulomb Barrier: Into the 21st Century, Yale, 1999.
[59] B. M. Nyakó, J. Gizon, D. Barnéoud, A. Gizon, M. Józsa, W. Klamra, F. A. Beck, and J. C. Merdinger, Z. Phys. A **332**, 235 (1989).
[60] N. Tajima, Nucl. Phys. **A572**, 365 (1994).
[61] A. A. Hecht *et al.*, Phys. Rev. C **63**, 051302(R) (2001).
[62] D. J. Hartley *et al.*, Phys. Rev. C **64**, 031304(R) (2001).
[63] L. L. Riedinger *et al.*, Acta Phys. Pol. B **32**, 2613 (2001).
[64] I. Hamamoto and B. R. Mottelson, Phys. Lett. **132B**, 7 (1983).
[65] G. Andersson *et al.*, Nucl. Phys. **A268**, 205 (1976).
[66] R. Bengtsson, H. Frisk, F. R. May, and J. A. Pinston, Nucl. Phys. **A415**, 189 (1984).
[67] G. B. Hagemann and I. Hamamoto, Phys. Rev. C **40**, 2862 (1989).
[68] D. J. Hartley *et al.*, Phys. Rev. C **65**, 044329 (2002).
[69] E. S. Paul *et al.*, Nucl. Phys. **A676**, 32 (2000).